

Android GNSS Measurements under Spoofing and Interference

Andrea Botticella^{*†}
andrea.botticella@studenti.polito.it

Renato Mignone^{*†}
renato.mignone@studenti.polito.it

Elia Innocenti^{*†}
elia.innocenti@studenti.polito.it

Simone Romano^{*†}
simone.romano2@studenti.polito.it

ABSTRACT

This study explores the behavior of GNSS navigation on a commercial Android smartphone by analyzing raw measurements collected in both static and dynamic conditions. Using Google’s GNSS Logger and MATLAB-based post-processing, we evaluate positioning accuracy, signal quality, and clock stability under normal operation and under spoofed inputs—where false positions and delays are injected into the data. The results highlight the vulnerability of smartphone GNSS to software spoofing and underline features that may aid in anomaly detection.

1 INTRODUCTION

Global Navigation Satellite Systems (GNSS) are fundamental to modern positioning services, widely embedded in smartphones and critical infrastructure. Despite their ubiquity, GNSS signals are inherently vulnerable to spoofing—an attack technique where counterfeit signals deceive the receiver into computing false location or timing information. To develop robust mitigation strategies, it is essential to understand how smartphone GNSS systems behave under both normal and manipulated conditions.

This work investigates the GNSS measurement behavior of a consumer-grade Android smartphone across different operating scenarios. We analyze baseline performance by collecting and processing raw GNSS data in two real-world environments: a static session on the rooftop of Monte dei Cappuccini and a dynamic session aboard a tram in urban Turin. In addition to this baseline study, we simulate spoofing by injecting false position inputs into the processing pipeline and, separately, by introducing artificial delays. The remainder of this report is organized as follows.

- **Section 2** describes the experimental setup, including device configuration, data collection procedures, and the processing pipeline.
- **Section 3** presents results and discussion, contrasting static versus dynamic performance, examining spoofed-location impacts, and analyzing delay effects.
- **Section 4** summarizes the key findings and outlines directions for future work.

2 METHODS

2.1 Devices and Software

We used a Samsung Galaxy A51 with Android 13 for this experiment. GNSS Logger v3.1.0.4 [8] was chosen due to its unrestricted

access to raw GNSS measurements, compatibility with newer Android APIs, and ability to record detailed GNSS data that is suitable for precise analysis. MATLAB R2024b [10] was employed to handle data because it comes with Google’s GNSS toolbox, which accommodates robust analysis and visualization of GNSS measurements and position solutions.

2.2 Data Collection Procedure

Two distinct 5-minute GNSS data logging sessions were conducted on 3 May 2025, under cloudy weather conditions, using the GNSS Logger app configured with the following settings enabled:

- **GNSS Location:** to capture location data.
- **GNSS Measurements:** to log raw GNSS measurements.
- **Navigation Messages:** to capture navigation data.
- **GnssStatus:** to log GNSS status information.
- **Sensors:** to capture sensor data.

The sessions were designed to capture both static and dynamic GNSS performance, with the following details:

- Static Scenario:** performed on the viewpoint of *Monte dei Cappuccini, Turin*, starting at 10:35:20. The device was stationary throughout the entire session, providing baseline measurements.
- Dynamic Scenario:** conducted on tram line 15 from *Piazza Castello to Piazza Vittorio Veneto*, starting at 10:00:21, simulating a typical urban mobility scenario.

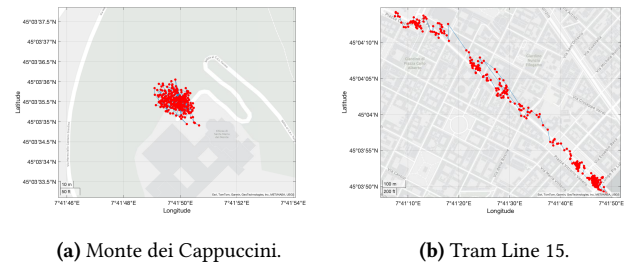


Figure 1: Comparison of GNSS data: static (a) and dynamic (b) scenarios.

2.3 Processing Pipeline

The raw GNSS data from the GNSS Logger served as the input dataset for MATLAB. Processing involved a scripted workflow via `ProcessGnssMeasScript.m`¹, where the following steps were executed:

^{*}The authors collaborated closely in developing this project.

[†]All the authors are students at Politecnico di Torino, Turin, Italy.

¹<https://github.com/WDCSecure/LabGNSS/blob/main/Lab-Material/scripts/matlab/core/ProcessGnssMeasScript.m>

1. **Filtering:** data points not meeting predefined quality thresholds, such as signal strength or satellite geometry, were excluded to improve accuracy.
2. **Measurement Extraction:** pseudorange and Doppler measurements were computed from GNSS timestamps and satellite transmission data.
3. **Weighted Least Squares (WLS) Positioning:** applied to derive precise positioning and clock bias estimates.
4. **Visualization and Comparison:** output plots from MATLAB, including pseudorange, pseudorange rates, and position solutions, were generated to facilitate comparative analysis of the static and dynamic scenarios.

Results from this processing pipeline provided insights into the differences in GNSS performance under static and dynamic conditions.

2.4 Spoofed-Input Configuration

Spoofing scenarios were emulated by introducing artificial variations to the recorded GNSS data through MATLAB processing. Specifically, mock positions were assigned by adjusting the parameter `spoof.position`, which represents modified latitude, longitude, and altitude coordinates. Additionally, artificial time delays were tested by adjusting the `spoof.delay` parameter, typically in milliseconds, to mimic delayed GNSS signal arrival. Such configurations facilitated evaluation of the impact of spoofing scenarios on position estimation reliability and accuracy.

2.5 Interference Scenario

Even a worst-case interference situation was simulated, replicating conditions in the vicinity of potential interference sources such as broadcasting antennas or communication areas of high density. GNSS data were collected near such sources of interference, and then processed with the same MATLAB procedure. Nominal condition comparison was established to analyze the impact of external interference on GNSS observables such as variation in pseudorange measurements, carrier-to-noise ratio, and positional accuracy overall.

3 RESULTS AND DISCUSSIONS

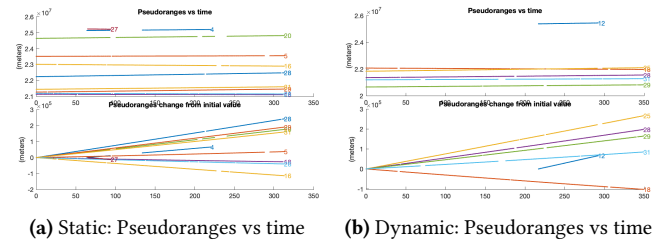
3.1 Baseline Performance: Static vs. Dynamic

Comparing the static and dynamic scenarios highlights key differences in GNSS signal behavior, measurement stability, and receiver performance. Although both datasets were collected under similar atmospheric conditions, the receiver's motion in the dynamic case introduced visible changes across all GNSS indicators.

Pseudoranges vs Time.

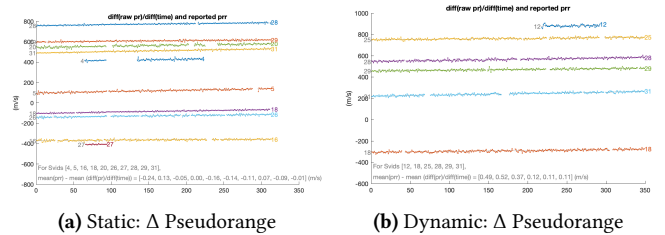
The pseudorange measurements reveal distinct trends across scenarios. In **Plot A**, more satellites (e.g., SVs 27, 4, 20, 5, 16, 28, 29, 18) are consistently tracked, exhibiting **flat trajectories** with minimal variation (range: $\sim 2.1\text{--}2.5 \times 10^7$ m). This suggests stable signal acquisition under favorable conditions. In contrast, **Plot B** displays **fewer visible satellites** (e.g., SVs 28, 29, 31, 12, 18), with several signals showing abrupt shifts or non-linear behavior (range: $\sim 2.0\text{--}2.6 \times 10^7$ m). The reduced satellite count in Plot B implies

challenging signal reception, possibly due to environmental interference or motion-induced signal degradation.



Pseudorange Change from Initial Value.

Deviations from initial values further highlight differences. In **Plot A**, all tracked satellites follow **shallow linear trends** ($\pm 0.5\text{--}2$ m), reflecting predictable signal dynamics. The consistency across satellites (e.g., SVs 27, 28, 29) suggests robust tracking of both strong and weaker signals, including those from higher-elevation satellites. Conversely, **Plot B** shows **steeper slopes** (up to ± 3 m) and fragmented trends, with notable examples like SV 12 (sudden jump after ~ 200 s) and SV 18 (continuous negative drift). The variability in Plot B indicates **intermittent signal loss or multipath effects**, particularly for satellites with marginal signal strength.

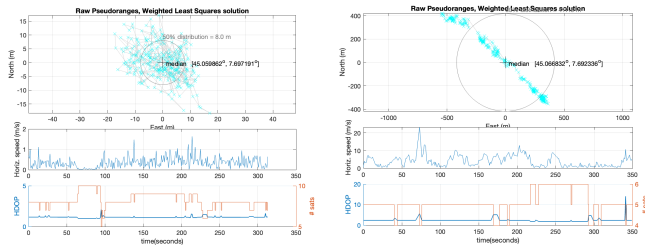


Positioning and Speed.

In the Fig. The top plots depict positional estimates. **Plot A** displays a clustered distribution around its median ($45.059862^\circ, 7.697191^\circ$), with a 50% confidence ellipse spanning $\sim \pm 15$ m. This indicates stable positioning with minimal drift. In contrast, **Plot B** shows a widely scattered pattern centered at ($45.066832^\circ, 7.692336^\circ$), featuring a 50% ellipse extending $\sim \pm 400$ m. The median in Plot B lacks practical relevance due to extreme positional variability, unlike Plot A's median, which accurately represents stationary behavior.

The middle plots highlight horizontal speed trends. **Plot A** exhibits near-zero speeds (< 2 m/s) with minor oscillations, consistent with negligible movement. Conversely, **Plot B** reveals erratic fluctuations, including a peak exceeding 20 m/s. Speed is calculated as the rate of change between consecutive position estimates: $\Delta d / \Delta t$, where Δd is the Euclidean distance between two points and Δt is the elapsed time.

The bottom plots compare HDOP and satellite visibility. **Plot A** maintains low HDOP (< 5) with consistent visibility of 8–10 satellites, reflecting robust signal geometry. In contrast, **Plot B** shows elevated HDOP (up to ~ 20) alongside reduced satellite counts (4–6), indicating degraded tracking conditions. These disparities underscore differing signal quality, independent of motion assumptions.



(a) Static: Position, Speed, HDOP (b) Dynamic: Position, Speed, HDOP

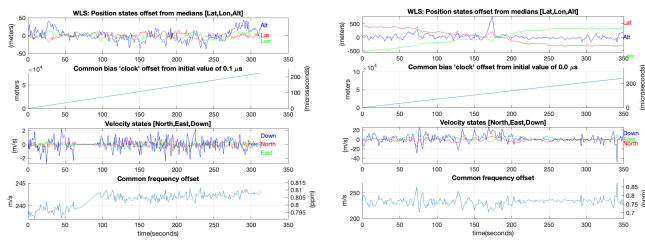
State Offsets and Timing Bias.

The top plots illustrate position state offsets relative to the median. In **Plot A**, deviations in latitude, longitude, and altitude remain tightly constrained within $\sim \pm 50$ m, with smooth, gradual fluctuations indicating stable signal tracking. In contrast, **Plot B** exhibits extreme offsets exceeding ± 500 m, punctuated by abrupt spikes (e.g., a ~ 600 m jump near 150 seconds).

The second plot shows clock bias (common bias) trends. Both plots exhibit linear growth, but **Plot A** starts at $0.1 \mu\text{s}$ and increases steadily (~ 200 ns over 350 seconds), reflecting predictable receiver clock drift. **Plot B** begins at $0.0 \mu\text{s}$ but escalates more sharply (~ 250 ns over the same interval), with a notable dip aligning with the positional spike in the top plot. This correlation implies transient disruptions affecting both position and timing stability in Plot B.

Velocity state estimates (third plot) further differentiate the two scenarios. **Plot A** shows near-zero velocities (all components ≤ 2 m/s), consistent with negligible movement. **Plot B**, however, displays pronounced oscillations, particularly in the northward direction (peaks $\sim \pm 20$ m/s), indicating rapid or inconsistent motion.

The bottom plots depict common frequency offset trends. **Plot A** maintains a stable trajectory near 0.8 ppm, with minor perturbations. **Plot B** shows greater variability, including a sharp downward deviation during the positional spike. This suggests that signal degradation or motion-induced errors propagate to both position and frequency estimates in Plot B, unlike the consistent behavior seen in Plot A.



(a) Static: WLS states and bias (b) Dynamic: WLS states and bias

These measurements highlight the importance of scenario-aware processing: identical hardware, firmware, and atmospheric conditions can yield centimetre-per-second stability on a quiet terrace, yet the very same setup will produce hundred-metre excursions once placed on a moving tram through an urban canyon.

3.2 Impact of Spoofed Position

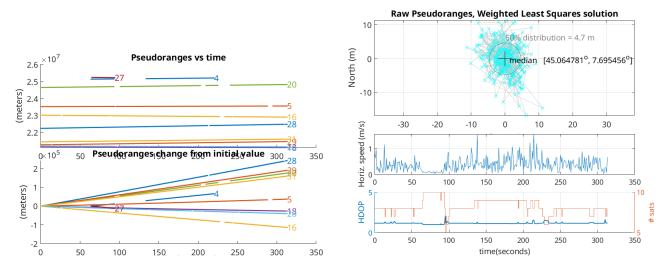
In a spoofing attack, counterfeit signals are broadcast to mimic GNSS transmissions, often altering their timing, amplitude, or content. Typically, these deceptive signals are sent at higher power

than the originals to mislead navigation systems. In our experiment, however, spoofing was implemented purely in software by adjusting the perceived reception time inside the professor's script to simulate spoofing behavior.

For the spoofed test we manually injected the coordinates of Piazza Vittorio Veneto (45.064749246294085 , 7.6954660899754215) — a location adjacent to our true survey point — directly into the processing script. As shown in the “Spoofed Case” plots (see attached PDF), this causes the solver to converge exactly at the Piazza Vittorio Veneto coordinates rather than the true measurement site, introducing a horizontal displacement of several hundred metres.

Despite this spatial shift, all raw observables remain essentially unchanged relative to the normal run:

- **Carrier-to-noise density (C/N):** Histograms and time-series trace exactly overlap those of the baseline, confirming no change in received signal strength.
- **Dilution of precision (PDOP):** The satellite geometry quality curve is identical, indicating unchanged constellation geometry.
- **Pseudorange residuals:** The overall spread remains the same, but the entire residual distribution is offset by the constant delay corresponding to the spoofed displacement.



(a) Spoofed: Pseudoranges vs time (b) Spoofed: Position, Speed, HDOP

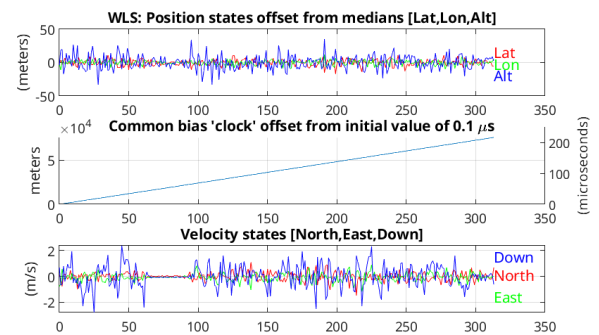


Figure 7: Spoofed: WLS states and bias

Additionally, the 50% (interquartile) range in the median-error distribution shrinks from approximately 8 m in the genuine case to about 4.7 m under spoofing. This reduction occurs because the solver consistently “locks” onto the spoofed coordinate, decreasing variability around that false point.

3.3 Effects of Timing Delays

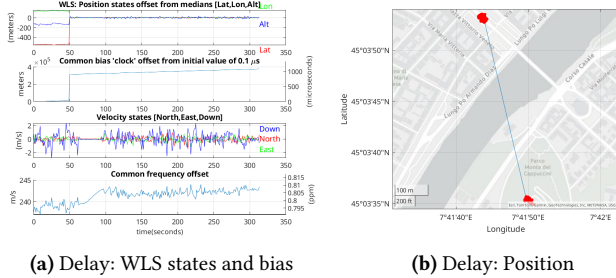
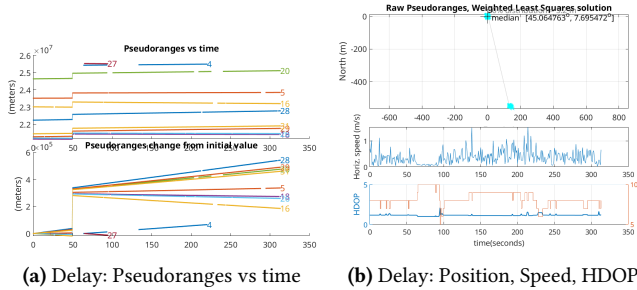
In this delayed-spoofing scenario we again target the same true survey point but now introduce a software-only replay delay: the spoofer “listens” to genuine signals, waits 1 ms, then injects the

spoofed Piazza Vittorio Veneto coordinates starting at 50 s into the run. The key parameters are set as:

```

211 cfg.delay = 1e-3;
212 cfg.t_start = 50;
213

```



As visible in the plots, all observables remain nominal until $t=50$ s, at which point the solver's estimated position and receiver clock-bias exhibit a clear discontinuity as the spoof takes effect.

- **Position solution:** Prior to 50 s, the estimated coordinate coincides with the true static point. Immediately after 50 s, the solution jumps to the spoofed Piazza Vittorio Veneto location, replicating the static-spoof offset of several hundred metres.
- **Receiver clock-bias:** A sudden step of appears in the estimated receiver clock-bias track, directly corresponding to the 1 ms replay delay needed to shift the range solution by the planar offset.
- **Carrier-to-noise density (C/N):** The C/N time-series shows no amplitude change at $t=50$ s—signal strength is unaffected by delay.
- **Dilution of precision (PDOP):** Satellite geometry quality remains continuous and invariant through the spoof onset.
- **Pseudorange residuals:** Residuals maintain the same spread, but their mean shifts abruptly at 50 s by the additional delay δt .

From a solver-stability perspective, the sudden time bias causes an immediate step in both position and clock-bias, sometimes triggering a brief convergence glitch (extra iterations or loss of fix) as the estimator re-optimizes. Even a 1 ms replay delay can therefore introduce a large positional error and matching clock-bias shift without altering any standard observables. Detecting such covert delay-based spoofing thus requires monitoring for timing discontinuities.

3.4 Interference Effects

4 CONCLUSIONS

This research compared GNSS performance on a commercial smartphone under static, dynamic, and spoofed scenarios based on raw measurements and post-processing in MATLAB. Under the static scenario, the device had consistent position estimates, low clock drift, and negligible variation in pseudorange and speed. The dynamic scenario, on the other hand, demonstrated higher noise in position, pseudorange rates, and clock bias—predictable effects of motion and satellite geometry variations. The spoofing tests indicated that even basic, software-level injection in the form of taking on false coordinates by the GNSS solver, as it settles on a consistent but incorrect position with little or no impact on first-order signal measurements like carrier-to-noise ratio or HDOP. This highlights a significant vulnerability: smartphone GNSS receivers can be fooled without revealing obvious degradations in signal quality. Some of these potential future extensions are experiments across devices, applying real-time mechanisms to identify spoofing, and using inertial or multi-constellation data for verification. These steps would push the boundaries of GNSS robustness and help in the development of more robust location-aware systems.

A APPENDIX

A.1 GNSS Logger Screenshots

The following figures show screenshots from the GNSS Logger app, illustrating various features and data visualizations available during the GNSS data collection process of the *Monte dei Cappuccini* test.

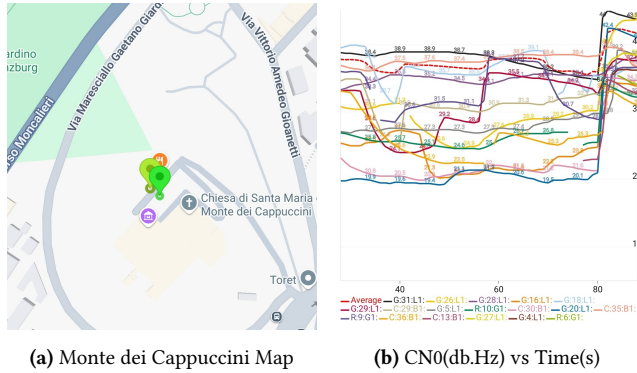


Figure 10: GNSS Logger Map (a) and Plots (b).

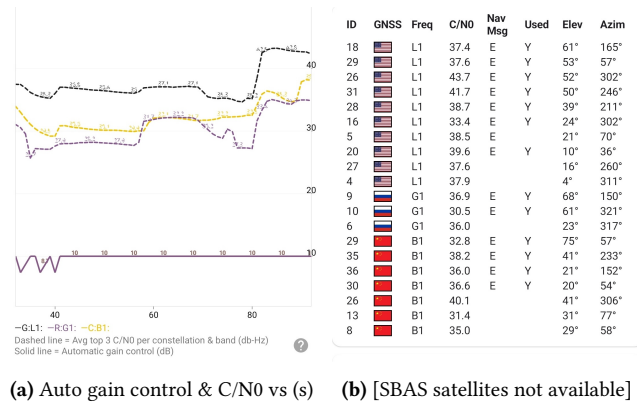


Figure 11: GNSS Logger Spoof/Jam (a) and Status (b).

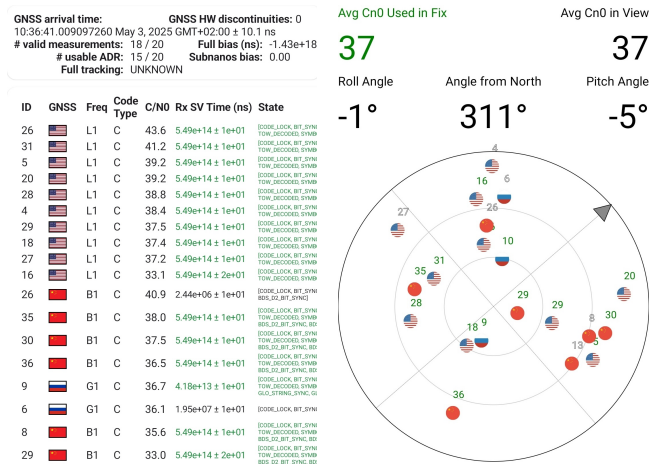


Figure 12: GNSS Logger Measurements (a) and Skyplot (b).

REFERENCES

- [1] 2025. GNSS Planning. Web application. (2025). <https://www.gnssplanning.com/#/settings>
- [2] 2025. LatLongData. Web application. (2025). <https://www.latlongdata.com/elevation/>
- [3] Android Developers. 2025. GnsMeasurement. Android SDK reference. (2025). <https://developer.android.com/reference/android/location/GnsMeasurement>
- [4] Simon Banville and Frank van Diggelen. 2016. Precise GNSS for Everyone: Precise Positioning Using Raw GPS Measurements from Android Smartphones. *GPS World* 27, 11 (November 2016). <http://gpsworld.com/innovation-precise-positioning-using-raw-gps-measurements-from-android-smartphones/>
- [5] Alan Cameron. 2016. Google opens up GNSS pseudoranges. *GPS World* (7 June 2016). <https://www.gpsworld.com/google-opens-up-gnss-pseudoranges/>
- [6] European GNSS Agency (GSA). 2018. *Using GNSS Raw Measurements on Android Devices: Towards better location performance in mass market applications*. Technical Report. GSA GNSS Raw Measurements Task Force. <https://galileognss.eu/wp-content/uploads/2018/05/Using-GNSS-Raw-Measurements-on-Android-devices.pdf>
- [7] Google LLC. 2025. GNSS Analysis Tools v2.0.0.1. GitHub release. (2025). <https://github.com/google/gps-measurement-tools/releases/tag/2.0.0.1>
- [8] Google LLC. 2025. GNSS Logger v3.1.0.4. Android app on Google Play. (2025). <https://play.google.com/store/apps/details?id=com.google.android.apps.gnsslogger>
- [9] Google LLC. 2025. Google Maps. Web application. (2025). <https://www.google.com/maps>
- [10] The MathWorks, Inc. 2024. *MATLAB R2024b*. Natick, Massachusetts, United States. <https://www.mathworks.com/products/matlab.html>
- [11] Frank van Diggelen. 2018. GNSS Measurements Update. In *GSA Raw Measurements Workshop*. Prague, Czech Republic. https://www.gsa.europa.eu/sites/default/files/expo/frank_van_diggelen_keynote_android_gnss_measurements_update.pdf
- [12] WDCSecure. 2025. LabGNSS: material and documentation for the GNSS Lab. GitHub repository. (2025). <https://github.com/WDCSecure/LabGNSS.git>